Supporting information

Effects of sintering temperature on thermoelectric figure of merit of trace Al_2O_3 doped n-type ZnO nanocomposites

Xizu Wang,*[,a] Yun Zheng,[a] Ady Suwardi,[a] Jing Wu,[a] Siew Lang Teo,[a] Qiang Zhu,[a] Gang Wu,*[,b] Jianwei Xu*[,a,c,d]

[a] Institute of Materials Research and Engineering (IMRE), Agency for Science, Technology and Research (A*STAR), #08-03, 2 Fusionopolis Way, Innovis, 138634, Singapore. Email: Email: jw-xu@imre.a-star.edu.sg; wangxz@imre.a-star.edu.sg
[b] Institute of High Performance Computing (IHPC), Agency for Science, Technology and Research (A*STAR), #16-16, 1 Fusionopolis Way, Connexis North Tower, 138632, Singapore Email: wug@ihpc.a-star.edu.sg
[c] Department of Chemistry, National University of Singapore, 3 Science Drive 3, Singapore 117543
[d] Institution of Sustainability for Chemical, Energy and Environment (ISCE2), 1 Pesek Road, Jurong Island, Singapore, 627833

Description: Supplementary Figures, Table and Notes

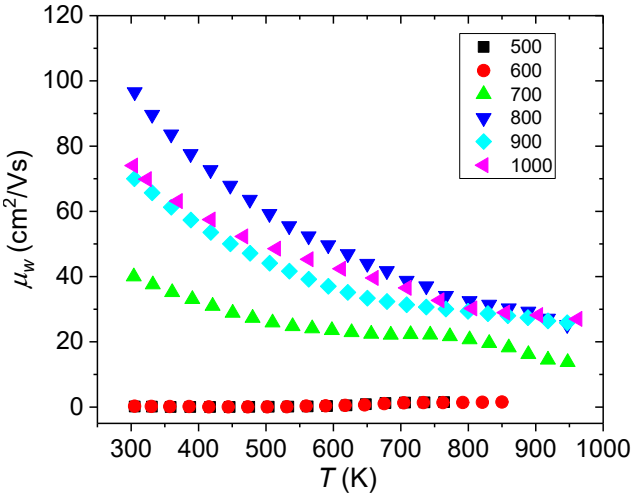

Figure S1. Calculated weighted mobility (intrinsic mobility) of AOZO nanocomposite as a function of temperature.

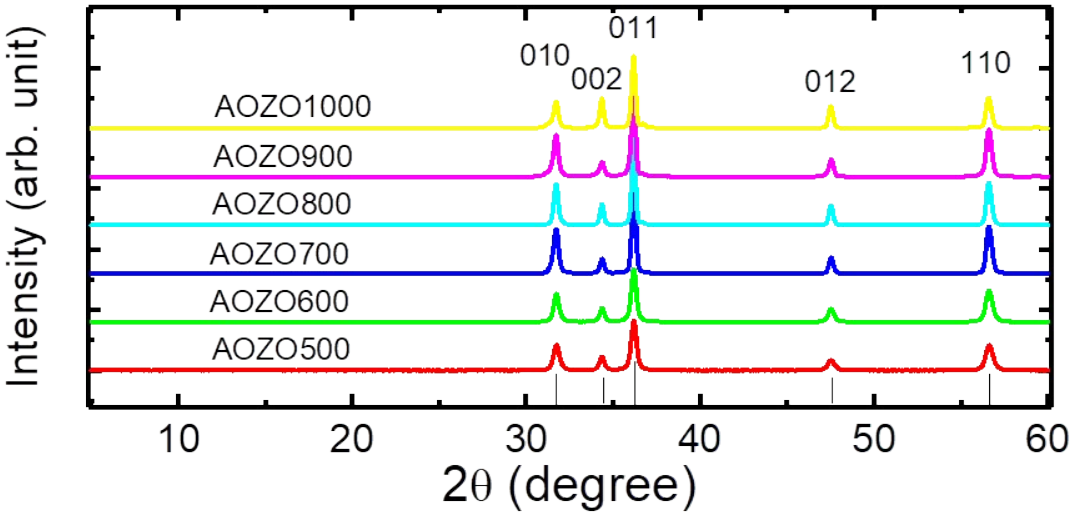

Figure S2. X-ray diffraction (XRD) patterns of AOZO under different sintering temperatures.

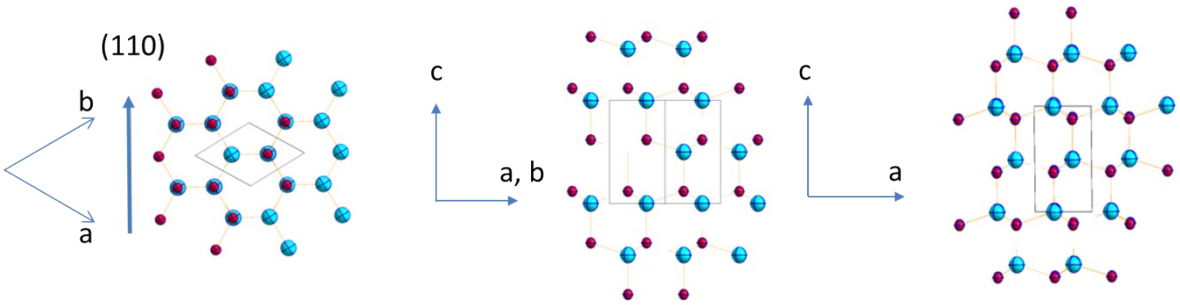

Figure S3. Crystal structure of AOZO based on XRD with different orientations. (Red dots: oxygen atoms; blue dots: metal atoms)

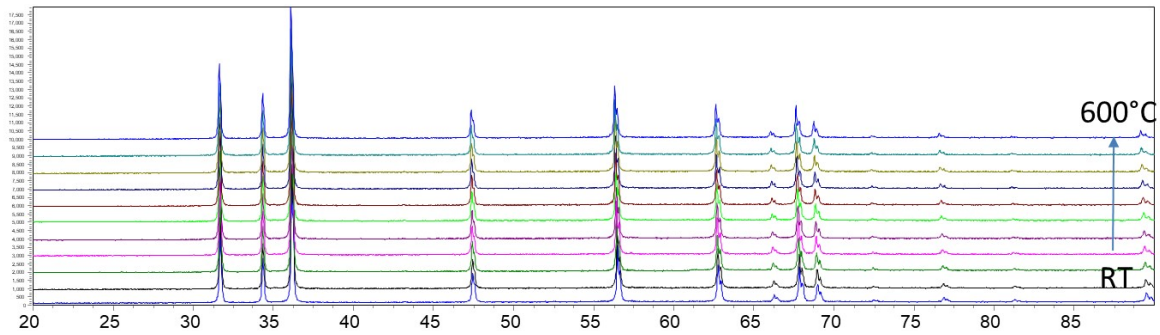

Figure S4. Temperature-dependent XRD patterns of AOZO700 pellets as a function of temperature.

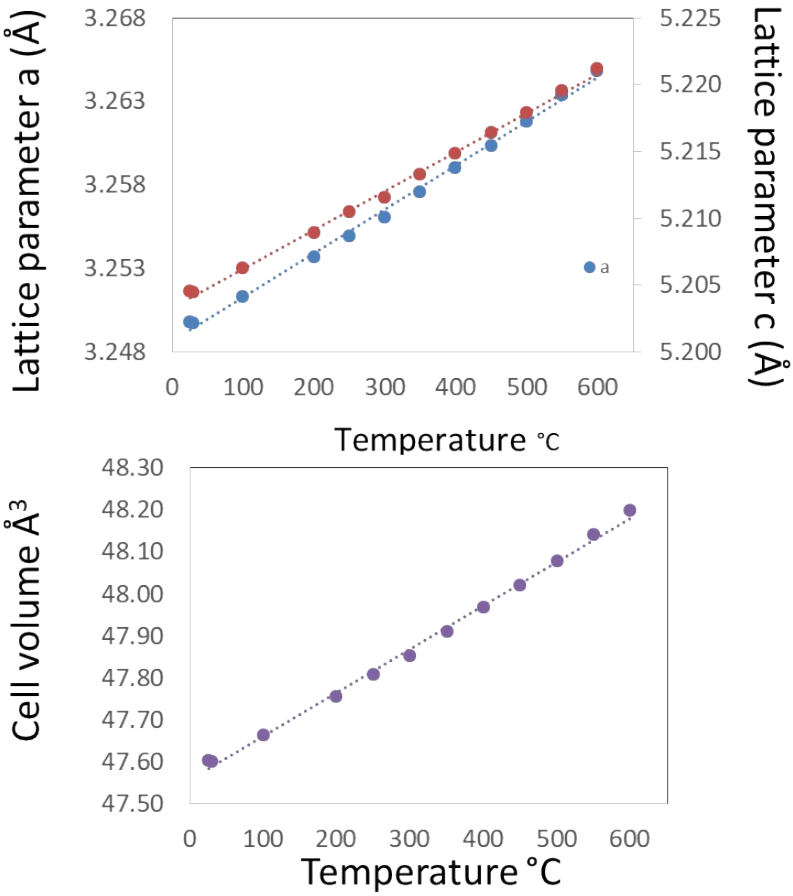

Figure S5. Calculated lattice parameters and cell volume of the AOZO700 based on its XRD data as a function of temperature.

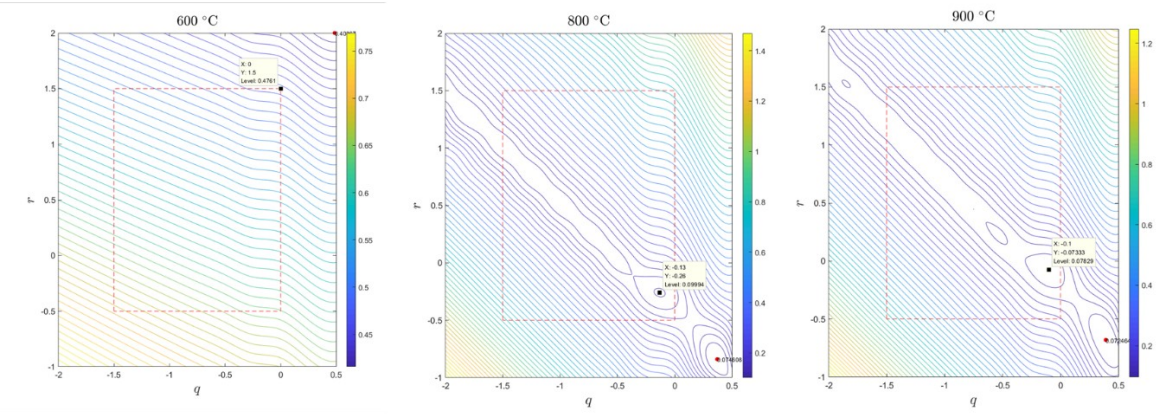

Figure S6. Carrier scattering fitting for AOZO600, AOZO800 and AOZO900, showing signs of optical phonon scattering, ionized impurity scattering and piezoelectric scattering dominated transport. The dots highlight the location of the best fitting. 'X' and 'Y' actually refer to q and r, respectively, while the 'level' refers to the error of the fitting. A smaller 'level' represents a better fitting.

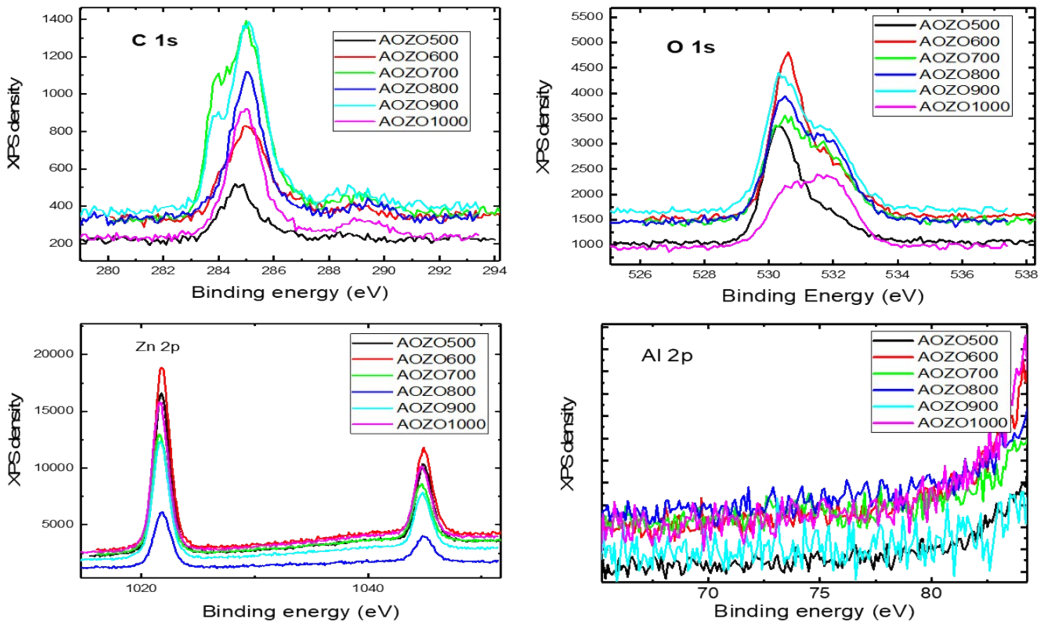

Figure S7. XPS spectra of AOZO.

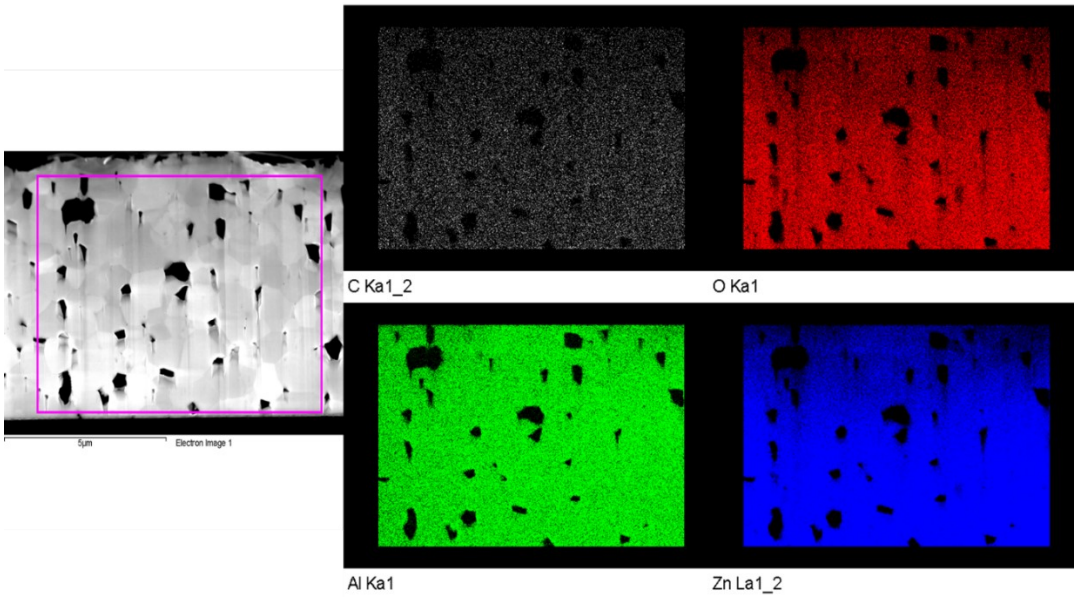

Figure S8. SEM image (left) and EDX of C, O, Al, Zn elements of AOZO700 (right)

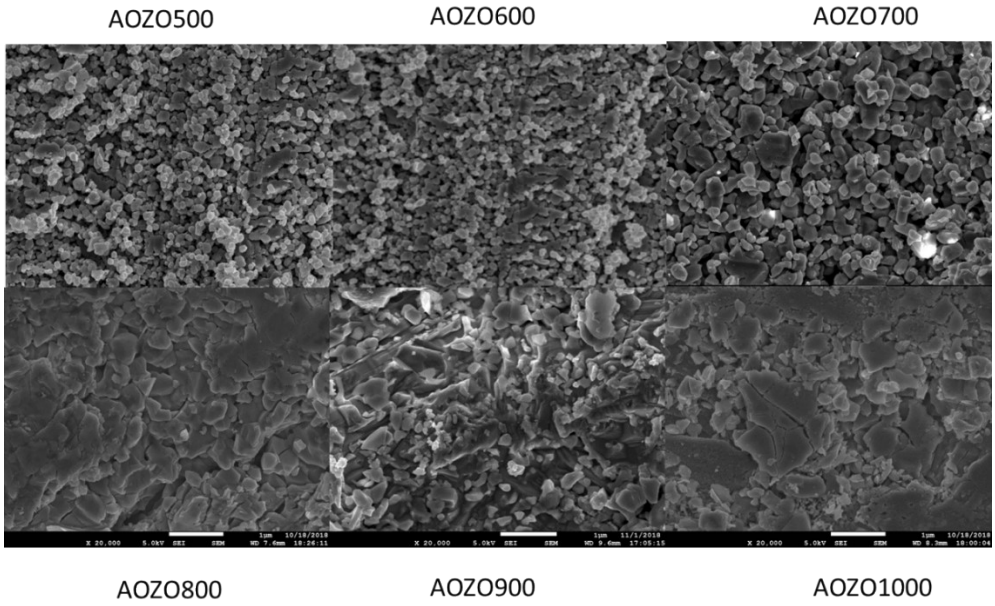

Figure S9. SEM images of samples AOZO500-1000

Modelling to determine the scattering mechanisms

In order to further understand the dominant scattering mechanism in AOZO, we developed a fitting procedure based on the Boltzmann Transport Equation (BTE) with the relaxation time assumption. [G. D. Mahan and J. O. Sofo, *Proc. Natl. Acad. Sci.* **1996**, *93*, 7436.]. Then the carrier concentration, conductivity and Seebeck coefficient can be expressed as

$$n = \int_0^\infty D(E) f dE \qquad \sigma = \frac{2q^2}{3m^*} \int_0^\infty \tau(E)\, E\, D(E) \left(-\frac{\partial f}{\partial E} \right) dE = \frac{2q^2}{3m^*} L^{(1)}$$

S , , and

$$= \frac{1}{qT} \frac{\int_0^\infty \tau(E) E D(E) \left(-\frac{\partial f}{\partial E} \right) (E - E_F) dE}{\int_0^\infty \tau(E) E D(E) \left(-\frac{\partial f}{\partial E} \right) dE} = \frac{1}{qT} \left[\frac{\int_0^\infty \tau(E) E^2 D(E) \left(-\frac{\partial f}{\partial E} \right) dE}{\int_0^\infty \tau(E) E D(E) \left(-\frac{\partial f}{\partial E} \right) dE} - E_F \right] = \frac{1}{q}$$

where $L^{(n)} = \int_0^\infty \tau(E)\, E^n\, D(E) \left(-\frac{\partial f}{\partial E} \right) dE$, $f = \frac{1}{1 + \exp\left(\beta(E - E_F)\right)}$, $\beta = \frac{1}{k_B T}$, and k_B is the Boltzmann constant. Given that we obtain the energy- and temperature-dependent relaxation time $\tau(E)$, we can calculate the transport properties by solving the above equations. Here, we assume that only one scattering mechanism is dominated, and thus the relaxation time can generally be written as $\tau(E,T) = \tau_0 \left(\frac{T}{T_0} \right)^q \left(\frac{E}{k_B T_0} \right)^r$, where $T_0 = 300$ K is arbitrarily chosen to make the temperature dimensionless. In the end, the temperature-dependent conductivity and Seebeck coefficients from BTE can be fitted to the experimental measurements, so that an appropriate set of parameters *q* and *r* can be estimated. Since *q* and *r* are distinct for different scattering mechanisms, the dominant scattering mechanism can be further identified by comparing their values with theoretical ones in Table S1. Therefore, this method provides is useful in understanding the underlying transport mechanisms.

We must emphasize that we assume that only one mechanism dominates the scattering, but it may not always be true. For example, in our AOZO700 – AOZO1000 samples, the best fitting can be obtained for a range of values, rather than a single point. In this case, we can expect several scattering mechanisms, rather than a single scattering mechanism, to determine the transport. In practice, we choose the several closest possible points matching the scattering mechanism in Table S1, and use them to interpret the scattering mechanisms.

AOZO700 is the most complex example in our analysis. Our fitting gives a minimum at q = -0.11 and r = 0.18, while there is no corresponding combination in Table S1. Because here q is approaching to "0", we can first look for the cases with q = 0. From Table S1, non-polar optical phonon (r = -0.5), polar optical phonon (r = 0 ~ 0.5), inter-valley optical phonon (r = -0.5), ionized impurity (r = 1.5), neutral impurity (r = 0), surface roughness (r = 0), and alloy (r = -0.5) are possible mechanisms. However, since AOZO is classified as an ionized oxide and thus a polar semiconductor, we can remove the contributions of inter-valley optical phonon, neutral impurity, surface roughness and alloy effect. Then we have non-polar optical phonon, polar optical phonon and ionized impurity as potential scattering mechanisms. Finally, because polar optical phonon usually contributes much stronger scattering than non-polar optical phonon to polar semiconductors, we keep only polar optical phonon (r = 0 ~ 0.5) and ionized impurity (r = 1.5) in our analysis for simplicity. Actually, the fitted r is 0.18, which is

closer to the polar optical phonon range, and hence the polar optical phonon effect is a more dominant scattering mechanism. Another possible (q, r) combination for AOZO700 is (-1, 0.97). According to Table S1, we can find the potential scattering mechanisms are acoustic phonon (r = -0.5) and piezoelectric effect (r = 0.5) when q = 1. For simplicity, we choose the nearest case, which is the piezoelectric effect. In the end, the scattering mechanisms for AOZO700 is a combination of polar optical phonon, ionized impurity and piezoelectric effect. Similar analysis was performed to other samples to determine the scattering mechanism.

Several important scattering mechanisms are given in Table S1, where the expression of scattering rates $\Gamma(k)$ were taken from references [Ferry, David K, *Semiconductor Transport* (1st ed.), London: CRC Press (2016); Lundstrom, Mark, *Fundamentals of Carrier Transport* (2nd ed.), Cambridge: Cambridge University Press (2000); Sheng S. Li, Semiconductor Physical Electronics, Springer-Verlag New York (2010)].

Table S1. Several important scattering mechanisms and the corresponding scaling parameters.

Scattering sources	$\Gamma(k) = \frac{1}{\tau(k)}$	q	r
Acoustic phonon	$\frac{D_A^2 k_B T (2m^*)^{\frac{3}{2}}}{2\pi\hbar^4 c_l} E_k^{1/2}$	-1	-0.5
Non-polar optical phonon	$\sqrt{\frac{m^*}{2}} \frac{m^* D_O^2}{\pi\rho\hbar^3\omega_0} \left[N_q\sqrt{E_k + \hbar\omega_0} + (N_q + 1)\sqrt{E_k - \hbar\omega_0} u_0(E_k -$	0	-0.5
Polar-optical phonon (weak screening)	$\frac{e^2\omega_O\left(\frac{1}{\varepsilon_\infty} - \frac{1}{\varepsilon(0)}\right)}{2\pi\hbar\sqrt{\frac{2E_k}{m^*}}} \left[\begin{matrix} N_0 \sinh^{-1}\left(\frac{E_k}{\hbar\omega_o}\right)^{\frac{1}{2}} + \\ (N_0 + 1)\sinh^{-1}\left(\frac{E_k}{\hbar\omega_o} - 1\right)^{\frac{1}{2}} \end{matrix}\right]$	0	0~0.5
Polar-optical phonon (strong screening)	(degenerated to non-POP)	0	-0.5
Inter-valley optical phonon	$\frac{\pi D_{if}^2 Z_f}{2\rho\omega_{if}} \left(N_i + \frac{1}{2} \mp \frac{1}{2}\right) g_{Cf}(E_k \pm \hbar\omega_{if} - \Delta E_{fi})$	0	-0.5
Piezoelectric (weak screening)	$\frac{m^* e^2 K^2 k_B T}{\pi\varepsilon_\infty\hbar^3 k} \left[\ln\left(1 + 4\frac{k^2}{q_d^2}\right) - \frac{4k^2}{4k^2 + q_d^2}\right]$	-1	0.5
Piezoelectric (strong screening)		-3	-1.5
Ionized impurity (weak screening)	$\frac{Z^2 e^4 m^*}{8\pi\varepsilon_\infty^2\hbar^3 k^3} \left[\ln\left(\frac{4k^2 + q_d^2}{q_d^2}\right) - \frac{4k^2}{4k^2 + q_d^2}\right]$	0	1.5
Ionized impurity		-2	-0.5

(strong screening)			
Neutral impurity	$\frac{20\varepsilon_\infty \hbar^3 N_n}{(m^* e)^2}$	0	0
Surface roughness	$\frac{2m^* \Delta^2 L^2 e^4}{\hbar^3 \varepsilon_s^2}\left(N_{depl}+\frac{n_s}{2}\right)^2\left[\frac{1}{\sqrt{1+k^2L^2}}E\left(\frac{k^2L^2}{1+k^2L^2}\right)\right]$	0	0
Alloy	$\frac{(\delta E)^2}{2\pi\hbar}\left(\frac{2m^*}{\hbar^2}\right)^{\frac{3}{2}}E_k^{1/2}$	0	-0.5

$\Gamma(k)$ is the scattering rate.

As usual, e and $\hbar$ are the elementary charge and the reduced Planck constant, respectively. The dispersion relationship is assumed to be parabolic at the band edge, i.e., $E_k = \frac{\hbar^2 k^2}{2m^*}$, where m^* is the effective mass and k is the carrier wave vector. With this parabolic dispersion, it is straightforward to obtain $g(E) \propto \sqrt{E}$ as the three-dimensional density of state at the energy E. D_A and D_O are the deformation constants of acoustic and optical phonons, respectively. ρ and c_l are the mass density and elastic constant, respectively. $N_q = \frac{1}{\exp\left(\frac{\hbar\omega_q}{k_B T}\right)-1}$ is the Bose-Einstein distribution function for the phonons. $\hbar\omega_0$ is the optical phonon energy. ε_∞ and $\varepsilon(0)$ are the high-frequency and static dielectric permittivities. The Debye wave vector $q_d = e\sqrt{\frac{n}{\varepsilon_\infty k_B T}}$ is the inverse of the screening length and controls the interaction range of the various Coulombic scatters.

For the intervalley scattering, D_{if} is the intervalley deformation potential which characterizes the strength of the scattering from the initial valley to the final valley, and $\hbar\omega_{if}$ is the intervalley phonon energy. Z_f is the number of final valleys available for scattering, and g_{Cf} is the density of states in the final valley. The term ΔE_{fi} is the difference between the bottom of the conduction bands in the final and initial valleys ($\Delta E_{fi} = 0$ for equivalent intervalley scattering). N_i is the number of intervalley phonons as given by the Bose-Einstein factor. K is an effective coupling constant for piezoelectric scattering. Piezoelectric scattering predominantly occurs at relatively low temperatures.

For impurity scattering(at low sintering temperature <600°C), the factor Z is inserted to account for the charge state of the impurity (normally $Z = 1$). N_n stands for the concentration of neutral impurities. For surface roughness scattering, the quantity Δ is the rms height of the fluctuation in the interface and L is the correlation length for the fluctuations. $E(x)$ is a complete elliptic integral of the second kind. ε_s is the effective dielectric constant across the

interface. N_{depl} and n_s are the charge concentrations in the depletion and inversion layers, respectively. For alloy scattering, the scattering potential δE represents the deviations from the virtual crystal model in a semiconductor alloy, and determines the electron scattering rate for alloy scattering directly. It is generally believed that the role of alloy scattering is very weak. In AOZO systems, the carrier density n is relatively low and the working temperature T is high, which means that q_d is generally small and the screening is weak.

Calculation of the weighted mobility (μ_W), the reduced Fermi level (η) and transport coefficient (σ_{E_0})

In addition, μ_W, η and σ_{E_0}were calculated based on the following equations (Jonson, M., and Mahan, G. D., Phys. Rev. 1980, B 21, 4223 & A Suwardi et al., Mater. Today Phys. 2020, 14, 100239.).

$$\sigma = \sigma_{E_0} \ln(1 + e^{\eta}) \tag{1}$$

$$S = \frac{k_B}{e}\left[\eta - \frac{(r+2.5)F_{r+1.5}(\eta)}{(r+1.5)F_{r+0.5}(\eta)}\right] \tag{2}$$

$$\sigma_{E_0} = \frac{e(2m_e k_B T)^{3/2}}{3\pi^2 h^3}\mu_W$$

Table S2. Summary of calculated weighted mobility (μ_W), the reduced Fermi level (η) and transport coefficient (σ_{E_0}) of AOZO.

Sample	σ_{E_0}(S/m)	η	μ_W (cm²/Vs)
AOZO500	5.4×10^1	5.7	1.7×10^{-1}
AOZO600	8.0×10^1	3.8	2.6×10^{-1}
AOZO700	1.0×10^4	7.7	3.2×10^1
	1.5×10^4		4.8×10^1
AOZO800	3.0×10^4	3.8	1.1×10^2
AOZO900	2.2×10^4	6.1	7.0×10^1
AOZO1000	2.3×10^4	11.2	7.4×10^1

Grain size and d-spacing calculation based on the XRD data

The *d*-spacings of the (010), (002), (011), (012) and (110) lattice planes were determined by Bragg's Law:

$$2dsin\theta = n\lambda$$

where d is the interplanar spacing, θ is the scattering angle, n is a positive integer and λ is the angle of the incident wave (λ = 0.154 nm for x-ray). The average grain size D was calculated by using Scherrer formula:

$$D = \frac{0.9\lambda}{\beta cos\theta}$$

where β is the full-width at half-maximum (FWHM) of the (002) peak. The parameter of XRD from the AOZO sample shown in Table S3.

Table S3. XRD parameter of AOZO.

Sample AOZO	a (Angstrom)	c	(010)	(002)	(011)	(012)	(110)	Grain size (nm)	Preferred	Less
500	3.24031(12)	5.19636(26)	2.80652	2.59857	2.476946	1.90676	1.62035	47.8(14)	(110)	
600	3.241490(82)	5.19686(18)	2.80797	2.5993	2.4706	1.90749	1.62118	53.4(12)	(110)	(002)
700	3.240276(76)	5.19181(17)	2.80617	2.59591	2.46865	1.90559	1.62015	89.2(27)	(110)	(002)
800	3.242027(78)	5.19587(17)	2.80764	2.5979	2.47008	1.90684	1.62099	93.0(30)	(110)	(002)
900	3.23793(10)	5.18740(24)	2.80425	2.59381	2.46689	1.90415	1.61897	63.2(19)	(110)	(002)
1000	3.24089(13)	5.19260(26)	2.80676	2.59639	2.46915	1.90596	1.62048	72.9(31)	(110)	(010)